ACS Sustainable Chemistry & Engineering

pubs.acs.org/journal/ascecg

Research Article

Jet Fuel Range Hydrocarbon Production from Propanal: Mechanistic Insights into Active Site Requirement of a Dual-Bed Catalyst

Isaac Yeboah, Xiang Feng, Gang Wang, Kumar Ranjan Rout, Zhenping Cai, Xuezhi Duan, Xinggui Zhou, and De Chen*

Cite This: *ACS Sustainable Chem. Eng.* 2020, 8, 9434−9446

Read Online

ACCESS | Metrics & More | Article Recommendations | Supporting Information

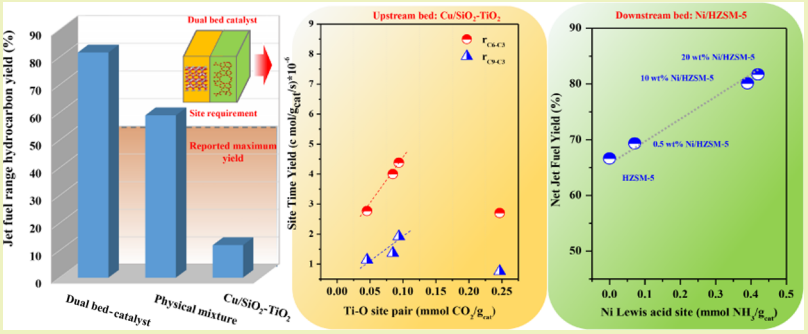

ABSTRACT: Utilization of sustainable biomass to produce jet fuel range hydrocarbons is imperatively needed to mitigate CO_2 emissions and to liberate the over-reliance on fossil resources. Using propanal as the feedstock, an excellent jet fuel range hydrocarbon yield (81.7%), high conversion (ca. 100%), and purity (85%) were achieved over a novel dual-bed Cu/SiO_2-TiO_2||Ni/ZSM-5 catalyst at low temperature and pressure in only one reactor. The intrinsic active site requirement was further investigated by multitechniques including density functional theory calculation, quantitative CO_2/NH_3-temperature-programmed desorption/diffuse reflectance infrared Fourier-transform spectroscopy, high-resolution transmission electron microscopy, and thermogravimetric analysis−mass spectrometry. Results showed that for the upstream bed catalyst (Cu/SiO_2-TiO_2), the Ti−O site pair and Ti Lewis acid site were crucial for enolate formation, carbon-chain growth, and ring closure reactions, which can be altered by the calcination temperature. The synergy between the site strength and number led to a volcanic relationship between acidity/basicity and the intermediate yield. In addition, the downstream bed Ni/HZSM-5 catalyst promoted the hydrodeoxygenation reaction toward hydrocarbon formation.

KEYWORDS: *jet fuel range hydrocarbons, active sites, tandem reaction, dual-bed catalyst, deactivation*

INTRODUCTION

Fuel and chemicals synthesized from sustainable biomass via pyrolysis to bio-oil and further catalytic upgrading harbor tremendous potential in the circular economy for future biorefinery practices.[1] This is urgently needed for biojet fuel production from the lignocellulosic biomass feedstock to meet the CO_2 emission reduction target. Fast pyrolysis of biomass following a catalytic vapor upgrading is a promising route for bio-jet and diesel fuels.[2] The high price of biofuels is now the main hurdle for the commercial applications,[3] and higher carbon yield is required to reduce the production cost of the biofuels. In the condensable compounds from the pyrolysis vapor or condensed bio-oil fractionations, there is a large fraction of small oxygenates containing aldehydes, ketones, alcohols, acids, furans, and anhydrosugars.[4] These compounds are very reactive and could be utilized to generate value-added chemicals. They can be separated from heavy fractions via aqueous phase extraction to decouple the complexity of bio-oil upgrading.[5] However, in the catalytic vapor upgrading, these oxygenates are normally hydrogenated to form light hydrocarbons, which lowers the carbon yield of biofuels and increases the production cost of biofuels.[6] Aldol condensation and ketonization of the light oxygenates can be applied to convert them to long-chain oxygenates,[7,8] where the aldol condensation reaction can increase the carbon number via intramolecular oxygen removal as water and simultaneous C−C coupling reactions. The resultant long-chain oxygenates can undergo a subsequent hydrodeoxygenation to yield fuel range hydrocarbons.[9,10]

Received: March 19, 2020
Revised: April 20, 2020
Published: May 12, 2020

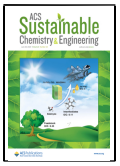

Because of the complexity, aldol condensation and/or ketonization and oxygen removal reactions usually take place in two cascading reactors as proposed by Dumesic et al.,[11] such as using Pd/ZrO_2 and $Pt/Al_2O_3-SiO_2$ in upstream and downstream reactors, respectively. Tandem reactions including aldol condensation, ketonization, and hydrodeoxygenation in one reactor could provide an attractive alternative for the production of low-cost biojet fuels. A dual-bed catalyst strategy can efficiently combine the different functions of catalysts, which is quite promising to fulfill the cascade reactions in only one single reactor at low temperatures to simplify the process.

Catalysts play a crucial role in the production of low-cost biofuels by catalytic fast pyrolysis processes. The catalyst activity, selectivity, and stability and the cost of catalysts have been identified as the main factors contributing to the production cost of biofuels.[6] Highly active, stable, and selective catalysts toward hydrocarbons with carbon numbers higher than 8 (i.e., C_{8+}) are essential for low-cost production of biojet and diesel fuels. However, the rational design of catalysts requires the fundamental understanding of the active sites and mechanistic insights for aldol condensation in tandem with hydrodeoxygenation. For the single bed catalyst, Iglesia et al.[12] first reported that Cu in the Cu/SiO_2-TiO_2 physically mixed catalyst is beneficial to improve the thermodynamic stability for condensation reactions.[10] They found that acidic-α hydrogen removal and the subsequent reaction between enolate and carbonyl could yield a chain growth intermediate, which rapidly dehydrates to form α-β-unsaturated enal or enone.[13−17] In addition, they also proposed that Ti^{4+} is used to stabilize enolates and the O^{2-} atom is used to aid in hydrogen abstraction. Even though the necessity of intermediate strength and site distance were pointed out as key factors for aldol condensation on TiO_2, the specific role and optimization of different acidic and basic site types and the corresponding relationship between acidic−basic sites and chain growth performance are still not clear.

When the oxygenate intermediate is formed, hydrodeoxygenation of oxygenates to aromatic hydrocarbon for jet fuel production requires both metal and acid sites for hydrogenation and oxygen removal to water[18] and aromatization,[19] respectively. Thus, hydrogenolysis, entailing hydrogenation and dehydration and further dehydrogenation to aromatics via hydrogen-transfer and trans-alkylation reactions, is of crucial importance.[7,20] Conventional HZSM-5 zeolites and their modified forms are known for the dehydration reaction via a strong Brønsted acidic function from the Al−O−Si framework.[21] The jet fuel range hydrocarbon yield can be 50% at 400 °C using the propanal feedstock.[8,22,23] However, the deactivation of HZSM-5 is severe because of coke formation.[24−26] Superior yield, as well as enhanced stability, requires the fundamental understanding of active site requirement, which is highly desired to facilitate the atom-economic and tandem conversion of light oxygenates to valuable hydrocarbons in the emerging biorefinery concept.

In this study, high yield (81.7%) and purity (85%) of jet fuel range aromatic hydrocarbons were obtained from propanal in one single reactor with a dual-bed configuration (Cu/SiO_2-TiO_2||Ni/ZSM-5) at low temperature and pressure, which offers a significant advantage over existing catalyst systems. The site requirement and reaction pathways for the conversion of light oxygenates were investigated by multitechniques including density functional theory (DFT) calculation, quantitative CO_2 and NH_3-diffuse reflectance infrared Fourier transform spectroscopy (DRIFTS)/temperature-programmed desorption (TPD), high-resolution transmission electron microscopy (HRTEM), thermogravimetric analysis−mass spectrometry (TGA-MS), Fourier transform infrared spectroscopy (FT-IR), N_2 physisorption, and X-ray diffraction (XRD). Active site strength and site numbers were manipulated by changing the calcination temperature of the TiO_2 catalyst and the Ni loading of the downstream HZSM-5 catalysts. The relation between the acid strength/type and jet fuel production rate was also elucidated. Moreover, the product stability, active sites, and reaction routes were also confirmed by the time-based analysis over 72 h. The fundamental insights into active sites unlock the potential to accommodate the structural complexity of the dual-bed catalyst system toward jet fuel production.

EXPERIMENTAL SECTION

Preparation of Catalysts. The upstream Cu/SiO_2-TiO_2 catalyst composed of the physical mixture of Cu/SiO_2 and TiO_2 with a weight ratio of 1:1. Cu/SiO_2 with a Cu loading of 5 wt % was synthesized by the conventional incipient wetness impregnation method, followed by drying overnight at 30 °C and calcination in air at 300 °C for 6 h dwelling time. The oxide catalyst was reduced at the same temperature in the presence of H_2 to yield the metallic Cu. The TiO_2 (P25) sample was purchased from Sigma-Aldrich (99.9%) and calcined in air (oxidative atmosphere) at different temperatures of 120, 350, 400, and 450 °C. The heating rate applied was 1 °C/min, and the dwell time was 4 h. NH_4ZSM-5 was purchased from Zeolyst International (CBV 3024E, SiO_2/Al_2O_3 = 30) and calcined at 500 °C for 6 h in static air (2 °C/min) prior to Ni impregnation. Ni/HZSM-5 (0.5 g) with Ni loading ranging from 0.5 to 20 wt % was also prepared by the incipient wetness impregnation method. The Ni-impregnated catalysts were calcined at 400 °C for 6 h in static air (2 °C/min) and reduced at 500 °C (10 °C/min) in a H_2 and N_2 flow of 50 mL/min and passivated in 1 wt % O_2 (50 mL/min) in helium at room temperature for 30 min.

Characterization of Catalysts. N_2 adsorption−desorption isotherms were determined on Micro metrics Trister 3000 at a liquid nitrogen temperature of 77 K for both fresh and spent catalysts. XRD measurements were taken using Bruker D8 ADVANCE (Cu Kα radiation, k = 0.15418 nm, 40 kV, 120 mA). HRTEM was performed on the JEOL JEM-2100F and JEM-ARM200F instruments operating at 200 kV. TEM examination of the spent catalyst was carried out using JEOL 2100, operated at 200 kV at the NTNU/SINTEF TEM Gemini Centre with an Oxford X-Max 80 EDX-instrument. For TPD experiments, 0.2 g of catalysts was used. In the TPD characterization, the TiO_2 samples were activated in helium (100 mL/min) at different temperatures by 10 °C/min increase and kept for 3 h. The TiO_2 samples calcined at different temperatures were named T120, T350, T400, and T450. For Ni/HZSM-5 catalysts, they were degassed for 1 h in flowing helium (200 mL/min) under the activation/reduction at 400 °C[10] and then cooled to 300 K for CO_2 adsorption and 100 °C for NH_3 adsorption, respectively.[18] Carbon dioxide was adsorbed on the reduced catalysts by exposure to 10 mol % CO_2 in helium (100 mL/min) for 30 min. Ammonia adsorption was performed in a similar manner as CO_2 adsorption, except that adsorption was done at 100 °C and a 1 mol % NH_3 in He gas mixture. Residual CO_2 and NH_3 were removed by purging the catalyst with helium (200 mL/min) at 35 and 100 °C for 2 h, respectively. Desorption of CO_2 and NH_3 was performed by heating the catalyst at a rate of 10 °C/min under flowing helium (50 mL/min) from 100 to 800 °C for NH_3 and 300 to 850 °C for CO_2. The Ni-based catalysts (HZSM-5, 0.5Ni/HZSM-5, 10Ni/HZSM-5, and 20Ni/HZSM-5) were reduced by flowing hydrogen (100 ml/min) for 2 h at 400 °C at a heating rate of 10 °C/min before TPD analysis. The signals of CO_2 (m/e = 44) and NH_3 (m/e = 17) were recorded by online MS and thermal conductivity detector (TCD). The quantification of the acid and the basic amount is based on a volumetric calibration of CO_2 and

https://dx.doi.org/10.1021/acssuschemeng.0c02200
ACS Sustainable Chem. Eng. 2020, 8, 9434−9446

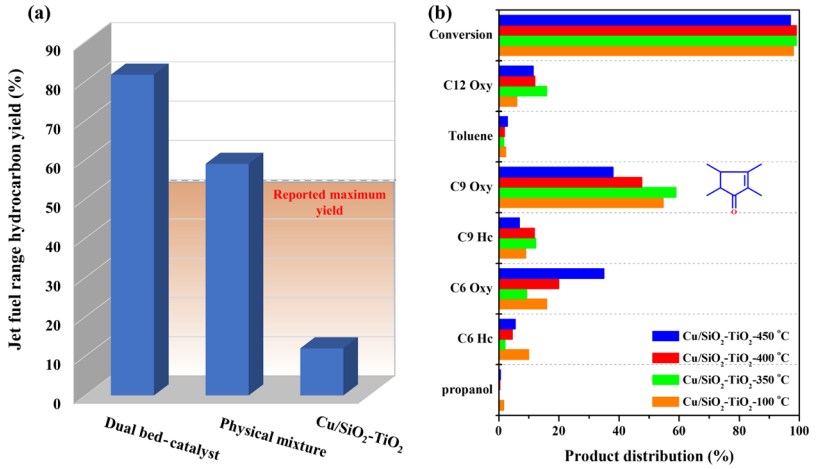

Figure 1. Jet fuel range hydrocarbon yield for a dual-bed Cu/SiO_2 (0.5 g)−TiO_2 (0.5 g)||Ni/HZSM-5 (1.0 g) catalyst and reported catalysts (a); carbon-based conversion and product distribution in the organic phase on the Cu/SiO_2−TiO_2 (0.5 g/0.5 g) catalyst at different calcination temperatures for aldol coupling of propanal (b). Reaction conditions: a temperature of 300 °C, 1/WHSV of 0.83 h based on the total weight of the catalyst, a propanal partial pressure of 0.63 bar, a hydrogen pressure of 0.22 bar, a total pressure of 1.0 bar, and a TOS of 5 h.

NH_3 adsorbed. The spent catalyst was characterized by TGA-MS using a Netzsch STA 4496 thermal analyzer system at a heating rate of 10 °C/min under the air atmosphere. The air and argon atmosphere was applied with a protective argon flow of 75 mL/min as well as an air flow of 25 mL/min. The IR spectra were recorded using a Nicolet iS50 IR spectrometer. All samples for the analysis were prepared and pressed in an evacuated die for 1 min. The data were obtained in an attenuated total reflection mode with a resolution of about 2 cm^{-1}. The CO_2/NH_3 absorption was explored by a DRIFTS experiment using a Nicolet Magna-11 550 spectrometer. For NH_3 and CO_2 DRIFTS, 0.08 g of sample was pretreated at 120 °C under argon for 2 h in a stainless chamber, followed by cooling down to 30 °C prior to recording the background spectrum. All the DRIFTS spectra were recorded at 30 °C with a spectral resolution of 8 cm^{-1} and an accumulation of 32 scans. Thereafter, the sample was exposed under 10% CO_2/Ar at 10 mL/min for 80 min or 7% NH_3/Ar at 10 mL/min for 50 min. The spectra were collected continuously during the process.

Catalytic Testing. In a typical process, 1.0 g of Cu/SiO_2−TiO_2 and 1.0 g of Ni/HZSM-5 of 100−150 mesh size were used as an upstream and downstream bed, respectively. The catalysts were tested in a fixed bed reactor with an inner diameter of 15 mm for all experiments at 0.1 MPa and 300 °C. Prior to the reaction, the upstream and downstream catalysts were reduced in situ with a 50% hydrogen in nitrogen at a total flow of 50 mL/min for 4 h at 300 and 400 °C, respectively. In dual-bed experiments, propanal liquid was fed to the reactor using a syringe pump N1000 with a typical flow of 0.48 mL/h for the dual-bed system. The feedstock (propanal, 0.63 bar, from Sigma-Aldrich, 99.9%) was mixed with hydrogen (0.22 bar, 99.9%) and nitrogen (99.9%) at the inlet of the reactor and flow into the catalyst bed. The reactant, gas phase, and condensed products were measured by gas chromatography (Agilent 6890) using a phenyl methyl siloxane capillary column (Agilent HP-5, 40 m, 320 μm ID, 0.25 μm film) connected to the FID/TCD detector and mass spectrometer (MSD 5977 E). Definitions of space velocity, propanal conversion, yield, and product selectivity are as follows: the WHSV is based on the total weight of the catalyst.

$$\text{WHSV} = \frac{\text{mass flow rate of feed (g/h)}}{\text{mass of catalyst (g)}} \quad (1)$$

$$\text{Conversion} = 1 - \frac{\text{mol of carbon of unconverted propanal}}{\text{propanal in organic phase}} \quad (2)$$

$$\text{Carbon based yield} = \frac{\text{mol of carbon in organic phase}}{\text{mol of carbon in feed}} \times 100\% \quad (3)$$

$$\text{Carbon based product distribution in organic phase} = \frac{\text{mol of carbon in a product}}{\text{mol of carbon in all products}} \times 100\% \quad (4)$$

$$\text{Purity} = \frac{\text{mol of jet fuel range hydrocarbon}}{\text{mol of all products in organic phase}} \times 100\% \quad (5)$$

Computational Details. DFT calculations were undertaken by the Vienna ab initio simulation package (VASP). Generalized gradient approximation based on the Perdew−Burke−Ernzerhof (PBE) formalism functional was used to calculate the electron exchange and correlation energy. The core electron interactions were determined by the projector-augmented wave method. An anatase TiO_2(101) cluster model was built because of its high thermodynamical stability and naturally exposed ability.[12] Bader charge analysis was implemented with a fast algorithm to determine the atomic charges of C, H, Ti, and O. The core charge density was used in the partitioning experiment.[27,28] The charge density difference of the propanal adsorption was calculated as $\Delta\rho(r) = \rho_{total}(r) - \rho_{surface}(r) - \rho_{oxygen}(r)$, where $\rho_{total}(r)$, $\rho_{surface}(r)$, and $\rho_{oxygen}(r)$ are the electron density of the whole adsorbed system, surface, and oxygen, respectively.

RESULTS AND DISCUSSION

Active Site for C_9-Cyclic Ketone Intermediate Formation from Propanal. Using propanal as the feedstock, the catalytic performance of the single bed Cu/SiO_2−TiO_2, dual-bed Cu/SiO_2−TiO_2||Ni/ZSM-5, and physically mixed catalysts were evaluated at low temperature (300 °C) and 0.1 MPa. Total conversions (100%) are observed for the three catalysts. However, the dual-bed catalyst shows a significantly boosted jet fuel range hydrocarbon yield (81.7%), better than the physical mixture catalyst (59.0%) and the single bed Cu/SiO_2−TiO_2 catalyst (12.3%), as shown in Figure 1a. This is mainly because there is a significant reduction of the gas-phase product yield from 27% (physically mixed catalysts) to 3.6% (dual-bed catalyst) and 1.3% (Cu/SiO_2−TiO_2) (Table S1, Supporting Information). In addition, the C_6−C_{12} oxygenates greatly decrease from 84% (Cu/SiO_2−TiO_2) to 14.7% (dual-bed catalyst) and 11.6% (physically mixed catalysts). The

https://dx.doi.org/10.1021/acssuschemeng.0c02200
ACS Sustainable Chem. Eng. 2020, 8, 9434−9446

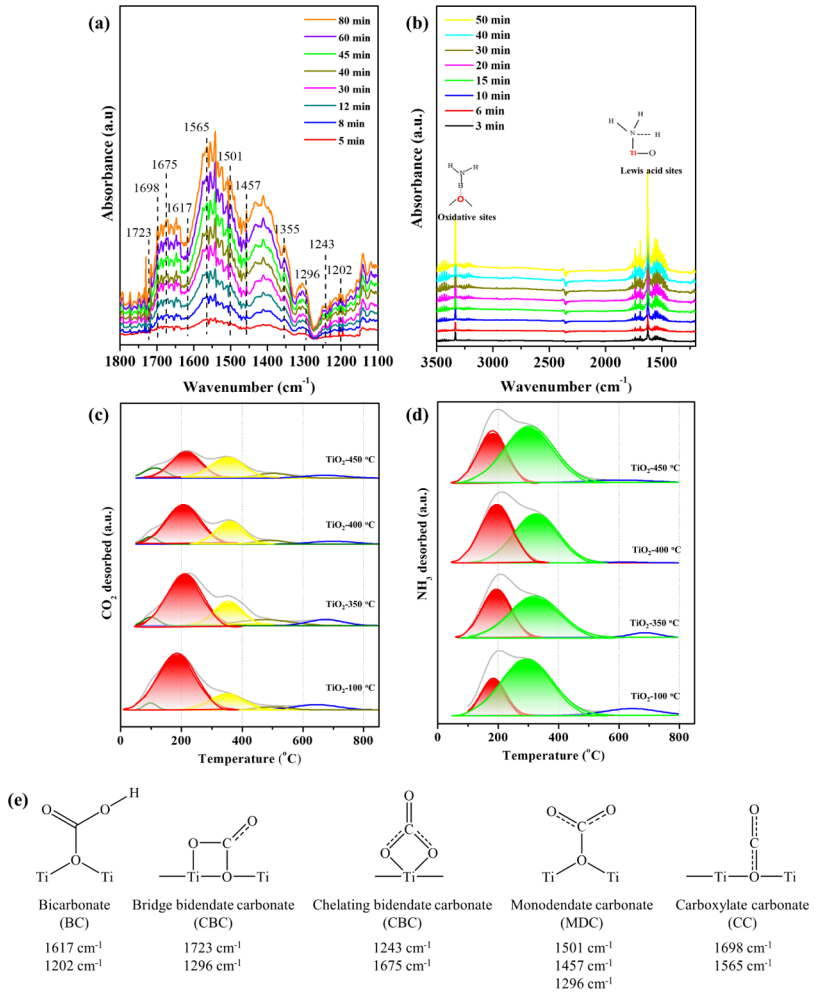

Figure 2. CO_2 (a,c) and NH_3 (b,d) DRIFTS and TPD spectra on TiO_2 calcined at different temperatures and (e) carbonate modes of adsorbed CO_2 species on TiO_2 (P25, calcined at 350 °C).

reason for the superior performance of the dual-bed Cu/SiO_2-TiO_2||Ni/ZSM-5 catalyst is that the propanal first contacts the upstream Cu/SiO_2-TiO_2 catalyst, yielding higher chain growth (mainly C_9 ketone) and preventing the side reaction (olefin generation via direct dehydration of propanal) over Ni/HZSM-5. It should be noted that the dual-bed catalyst also shows better performance than the reported catalysts in terms of jet fuel yield.[8,22,23]

To elucidate the intrinsic active sites, the upstream bed (Cu/SiO_2-TiO_2) and downstream bed (Ni/HZSM-5) catalysts were investigated separately. It was previously reported by Iglesia et al. that Cu/SiO_2-TiO_2 showed good aldol condensation performance.[12,29] The TiO_2 sites with acidic and basic sites are active toward aldol condensation, and Cu sites with a hydrogenation function can improve the forward reaction, making aldol coupling irreversible and preventing the prevalent thermodynamic obstacles in the aldol reaction.[10] However, there are distinct acidic and basic sites on TiO_2, and the intrinsic requirements for this reaction are still not clear. Therefore, the different active sites for the condensation reaction were manipulated by varying the passivation temperature of TiO_2 to modify the surface Lewis acid and basic site properties of the catalyst.

The physicochemical properties of the dual-bed Cu/SiO_2-TiO_2||Ni/ZSM-5 catalyst were first characterized by XRD and N_2 physisorption (Supporting Information, Figures S1 and S2). The XRD patterns (Figure S1) of the upstream Cu/SiO_2-TiO_2 catalyst have Cu(111), (200), and (220) peaks located at 43, 50, and 70°, respectively, indicating the Cu polycrystallinity character (PDF 00-044-0706).[30,31] For TiO_2 calcined at different temperatures, they exhibited similar phases, such as anatase phase at 25, 48, and 65° (PDF 00-002-0387) and rutile peaks at 27, 36, and 55° (PDF 00-002-0494).[32] The results suggest that the calcination at relatively low temperatures does not change the material phase. In addition, the XRD pattern of the downstream Ni/HZSM-5 coincides with the reported typical MFI structure of ZSM-5, and Ni(111) and Ni(200) are observed at 45 and 52°, respectively (PDF 04-016-1090).[33−35] With the increase of Ni loading, the Ni peaks are more intense. Figure S2 shows the porous structures of different catalysts. According to the IUPAC classification, the isotherms of samples show that HZSM-5, SiO_2, and TiO_2 are microporous, mesoporous, and nonporous materials, respectively. Moreover, part of Cu and Ni could reside in the pores of the support, as confirmed by the decrease of the pore volume.

The effect of calcination temperature of TiO_2 (P25) on the conversion and product distribution in the propanal coupling is illustrated in Figure 1b. The nearly complete conversions are observed by all the Cu/SiO_2-TiO_2 catalysts calcined at different temperatures (100, 350, 400, and 450 °C). The net product selectivity for secondary C_9 oxygenates[17] (2,3,4,5-

https://dx.doi.org/10.1021/acssuschemeng.0c02200
ACS Sustainable Chem. Eng. 2020, 8, 9434−9446

Table 1. Physico-Chemical Properties of the TiO_2 Catalysts from CO_2/NH_3-TPD

	basic sites modes					acidic sites		total sites (mmol/g)	
catalysts	BC	CBC (Ti)	BBC (Ti−O)	MDC	CC	O−H stretching vibration of oxygen site	Ti^{2+} Lewis acidity site	basic	acidic
TiO_2-100 °C	0.010	0.247	0.064	0.011	0.025	0.06	0.46	0.36	0.51
TiO_2-350 °C	0.007	0.094	0.039	0.017	0.011	0.02	0.26	0.17	0.28
TiO_2-400 °C	0.006	0.085	0.036	0.007	0.008	0.00	0.23	0.15	0.2
TiO_2-450 °C	0.008	0.029	0.025	0.006	0.004	0.00	0.17	0.11	0.18

tetramethyl-2-cyclopenten-1-one, 2,3-dimethyl-1,3-heptadiene, 2,4-dimethylheptanal, and propyl-2-methyl valerate) show a volcanic relationship with the calcination temperature. The corresponding carbon-based yields are 55, 59, 48, and 38% for TiO_2 calcined at 100, 350, 400, and 450 °C, respectively. The optimum product distribution is obtained at a calcination temperature of 350 °C. Besides C_9 oxygenates, the primary product is C_6 oxygenates (2-methyl-pentanal, 2-methyl-pentenal, and propyl propanoate) formed via aldol condensation and esterification pathway from propanal through the enolate intermediate mechanism.[7] The amount of Cu/SiO_2 remained constant based on the earlier work of Iglesia et al.[12] Figure 1b clearly shows that the calcination temperature of TiO_2 significantly changes the product yield. The effects of calcination temperature on the catalyst properties are then probed using CO_2 and NH_3-DRIFTS/TPD.

Normally, the adsorption of propanal and the formation of enolate require bifunctional Lewis basic and acid site pairs.[12,13] The basic and acidic properties of TiO_2-350 °C were examined using CO_2 and NH_3-DRIFTS, respectively. TiO_2 is a reducible metal oxide made of Ti^{4+} cations (Lewis acid sites) and O^{2-} anions (Lewis basic sites) on the surface and in the bulk. Therefore, CO_2 is either adsorbed on the oxygen or titanium atoms known as basic and acidic sites, respectively,[36] because the oxygen atoms of CO_2 are weakly basic, while the carbon is acidic. Figure 2a shows the CO_2-DRIFTS results from the TiO_2-350 °C sample pretreated under Ar at 120 °C and exposed to the CO_2/Ar mixture at 30 °C from 2 to 80 min. The increased intensities are attributed to the increased amount of the adsorbed species on the TiO_2 surface and gas-phase CO_2 in the diffuse reflection chamber. The observed bands in Figure 2a are consistent with the previously reported results,[37−41] where the bicarbonates (BCs): 1617, 1202 cm^{-1}; bridge bidentate carbonates (BBCs): 1296, 1723 cm^{-1}; chelating bidentate carbonate (CBC): 1243, 1675 cm^{-1}; monodentate carbonate (MDC): 1501, 1457, 1296 cm^{-1} and carboxylate carbonate (CC): 1565, 1698 cm^{-1} are observed, and their structures are shown in Figure 2e. The formation of BC requires interaction between CO_2 and TiO_2 surface OH (weak base site); CBC and BBC require participation of either adjacent cationic site and surface oxygen or both (Ti^{4+}−O^{2-}),[36,37] and finally, MDC and CC require one surface oxygen (O^{2-}, strong base sites). The identified DRIFTS peaks illustrate the active sites evolved with different strengths, as equally reported by León and Faba et al. BC represents weak acid pairs,[37,42] MDC and CC represent strong acid pairs, and CBC and BBC represent medium-strength acid−base pairs.

Furthermore, the acidic site's type for TiO_2-350 °C was also examined by NH_3-DRIFTS. The NH_3-DRIFTS adsorption mode on reducible metal oxide can be classified into (i) H-bonded NH_3 on oxidative sites: 3310 and 3396 cm^{-1}; (ii) Lewis acid-bonded NH_3: 1550 and 1600 cm^{-1}; and (iii) Brønsted acid-bonded NH_3: 1410, 1420, and 1680 cm^{-1}.[43] In Figure 2b, two major peaks are observed at a lower frequency (1500−1700 cm^{-1}) and higher frequency (3200−3500 cm^{-1}) representing the bending mode and N−H and O−H stretching vibration between H from NH_3 and surface oxygen, respectively. No peak is observed for Brønsted acid sites.[44] Furthermore, CO_2-TPD and NH_3-TPD were then used to determine the site's quantities and strength of the basic/acidic sites on TiO_2. The TPD curves are deconvoluted by the best model fitting to the Gaussian distribution.

Figure 2c,d illustrates the deconvoluted spectra of CO_2-TPD and NH_3-TPD for TiO_2 calcined at different temperatures. The CO_2 desorption profile strength in Figure 2c can be grouped into three major regions: weak (50−150 °C, BC), moderate [200−400 °C, bidentate (bridge and chelating)], and strong (>400 °C, monodentate and carboxylate) according to previous works.[45−47] The weak basic site is ascribed to BC with a peak maximum within 100−150 °C. This weak peak shifts to higher temperatures as the calcination temperature increases. The thermal stability order of adsorbed CO_2 species on TiO_2 is CC) ≈ MDCs > BBCs > CBCs ≈ BCs.[38] The medium basic sites were dominant and ascribed to (i) BBC (Ti−O) and (ii) CBC (Ti) on metal cations.[42,48−50] Finally, two minor peaks representing the strong basic site were observed as MDC and CC at ca. 500 and 650 °C, respectively. The detailed site counts for the samples based on TPD are summarized in Table 1.

Based on the site number obtained from the TPD results in Table 1, the dominating site pair is medium site form, that is, Ti and Ti−O sites on TiO_2 surfaces, which is in accordance with the literature.[12] It can be seen from Table 1 that the bridge (BBC, Ti−O) and chelating (CBC, Ti) bidentate sites on TiO_2 calcined at 100 °C showed the basic site amount of 0.247 and 0.064 mmol/g_{cat}, respectively. The determined site ratio for Ti/Ti−O decreases from 3.9 and remains stable at 2.4 and drops to parity at 1.2 ratios for TiO_2 calcined at 100, 350, 400, and 450 °C, respectively. This reveals that the Ti sites are dominating in TiO_2 (p25) at low calcination temperatures, while Ti−O is formed at the higher calcination temperatures. This agrees well with the reported observation that Ti−OH groups are converted to Ti−O in the anatase phase as the temperature increases and consistent with the reported thermal stability of adsorbed CO_2 on oxides such as TiO_2.[51,52] Furthermore, Figure 2d shows NH_3-TPD for the TiO_2 catalyst calcined at different temperatures. As inferred from NH_3-DRIFTS, the two intense chemisorbed peaks are Ti Lewis acid sites and O−H stretching vibration from the surface oxygen.[53] The lower temperature peak at about 200 °C originates from the physisorbed NH_3 or ammonium ions,[54] and the desorption peak at 350 and 650 °C is ascribed to Ti Lewis acid sites and O−H stretching vibration from the surface oxygen, respectively.[44] The determined Ti Lewis acid site count (Table 1) decreased from 0.46 to 0.17 mmol/g_{cat} with increasing temperature from 100 to 450 °C. The Ti Lewis acidic sites

https://dx.doi.org/10.1021/acssuschemeng.0c02200
ACS Sustainable Chem. Eng. 2020, 8, 9434−9446

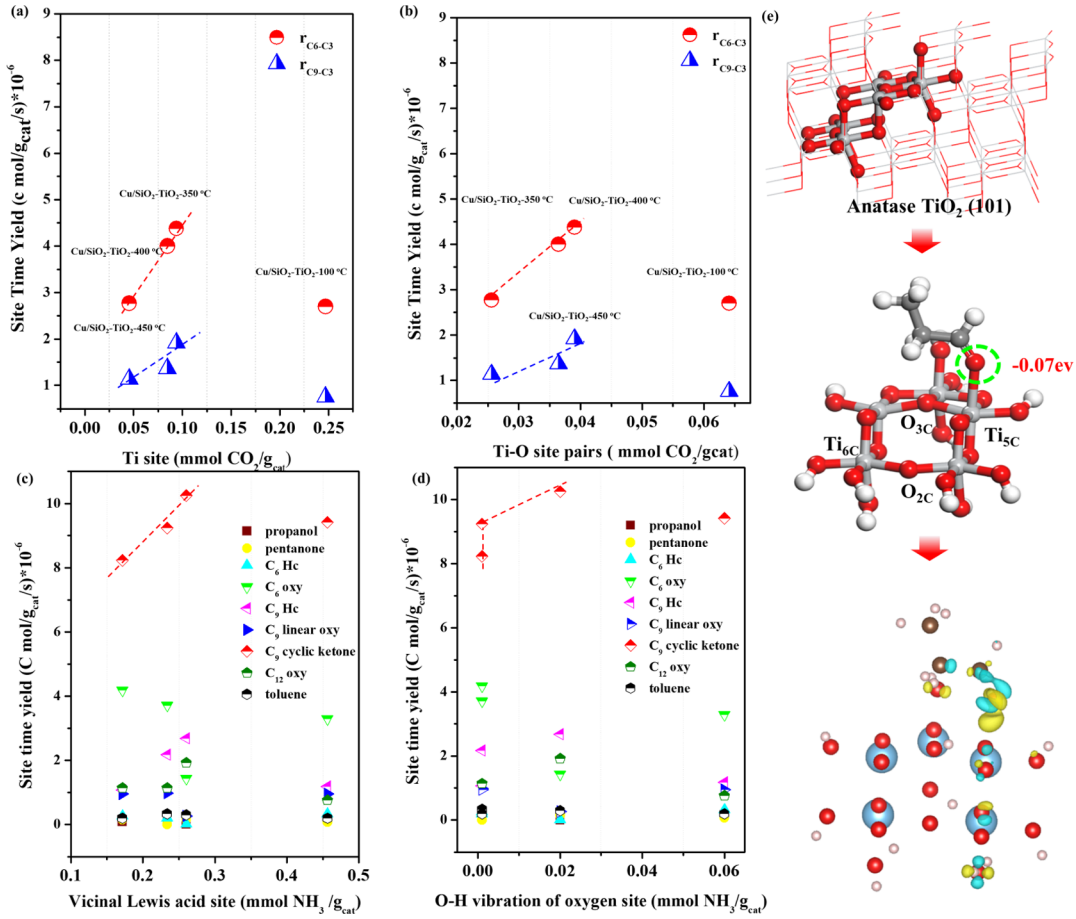

Figure 3. Net $r_{C_6-C_3}$ and $r_{C_9-C_3}$ site time yield as a function of the (a) number of Ti, (b) Ti−O site pairs, and site time yield as a function of (c) vicinal Lewis acid sites (Ti^{4+}) and (d) O−H stretching vibration of the oxygen site over Cu/SiO_2-TiO_2 catalysts. Reaction conditions: a temperature of 300 °C, 1/WHSV of 0.83 h, a propanal pressure of 0.63 bar, a H_2 partial pressure of 0.22 bar, a total pressure of 1.0 bar, and a TOS of 5 h. (e) DFT calculation of propanal adsorption and Bader charge analysis on $TiO_2(101)$.

account for over 89% of all acidic sites. This reduction in the Lewis acid sites is congruent to total surface area declines as the calcination temperature increases. Therefore, the total accessible site for NH_3 titration also decreases and resulted in a decline in the total sites with respect to the increase in the calcination temperature.

The catalytic consequence of the catalyst properties varied by the calcination temperature for the C−C coupling reactions of propanal via aldol condensation was then analyzed by correlating the number of the Ti and Ti−O sites to the catalytic performance. Based on product distribution in Figures 1 and 3 and also the results of Iglesia,[12] the simplified reaction pathways including the chain growth and termination steps are proposed and presented in Scheme 1. C_n^* represents the surface intermediate with a carbon number of n (n = 3, 6, 9, 12). C_n oxygenates and C_n hydrocarbons are the lumped oxygenates (including aldehydes, alcohols, and ethers) and hydrocarbons (including alkenes and alkanes) with the carbon number of n. r_{O_n} and r_{H_n} are the formation rate of the lumped oxygenates and hydrocarbons. For the chain growth, the adsorbed propanal first undergoes chain growth via self-condensation through C_3-enolate to yield C_6. The as-formed C_6 further undergoes cross-condensation with C_3-enolate to yield C_9. Finally, C_{12} oxygenates[17] are formed from cross-condensation between C_3-enolate and formed C_9. Herein, the subsequent cyclization reaction of linear oxygenates to cyclic

Scheme 1. Chain Growth and Termination Pathways in Propanal Conversion, Where C_n (n = 3, 6, and 9) Represents the Carbon Chain with n Carbon; r_{O_n} and r_{H_n} Represent the Molar Formation Rate (Site Time Yield) of C_n Oxygenates; and r_{H_n} Denotes the Dehydration−Hydrogenation or Hydrogenolysis Formation Rate of C_n Hydrocarbons; [C_3] and [H_2] Stand for the C_3 Intermediates and Hydrogen; Solid and Dashed Arrows Represent Carbon Chain Growth and Chain Termination, Respectively

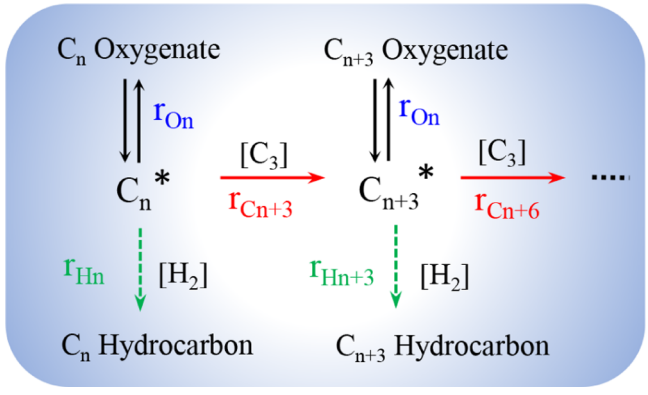

https://dx.doi.org/10.1021/acssuschemeng.0c02200
ACS Sustainable Chem. Eng. 2020, 8, 9434−9446

ketone results in a higher yield of C_9 ketone and thereby terminates the chain growth. For each intermediate, two steps terminate the products either through C_n oxygenates via desorption or C_n hydrocarbons via hydrodeoxygenation.

The chain growth rates of C_3 self-condensation and cross-condensation of C_6 and C_9 chains, namely, $r_{C_3-C_3}$, $r_{C_6-C_3}$, and $r_{C_9-C_3}$, can be obtained from the formation rates of individual compounds in eqs 6−8. The coefficients in equations represent the stoichiometric requirements for each one of these condensation steps.

$$r_{C_3-C_3} = r_{C_6} + \frac{6}{9}\left(r_{C_9} + \frac{9}{12}r_{C_{12}}\right) \quad (6)$$

$$r_{C_6-C_3} = r_{C_9} + \frac{9}{12}r_{C_{12}} \quad (7)$$

$$r_{C_9-C_3} = r_{C_{12}} \quad (8)$$

where r_6, r_9, and r_{12} are the formation rates of lumped oxygenates and hydrocarbons with a carbon number of 6, 9, and 12, respectively. It should be noted that r is the site time yield rather than a truly kinetic rate used in the present work.

To elucidate the requirement of the active site for the reaction, $r_{C_6-C_3}$ and $r_{C_9-C_3}$ were correlated to the dominating sites, that is, Ti (CBC) and Ti−O (BBC) site numbers, as shown in Figure 3a,b, respectively. In Figure 3a,b, the rates linearly increase with increasing number of Ti and Ti−O sites until reaching their maximum values of 350 °C calcination temperature for $r_{C_6-C_3}$ and $r_{C_9-C_3}$.

The results in Figure 3a,b suggest that both sites are required for the carbon coupling reactions. The Ti pairs are involved in the chain growth step by stabilizing the enolate for the surface reaction between enolate and adsorbed propanal. The kinetic relevant step of the reaction, according to Iglesia et al., involves the step for enolate formation from propanal. This step requires Ti−O pair where O in TiO_2 abstracts the acidic hydrogen at the alpha position in propanal.[12] Because the main product of our results is C_9 whose formation involves the Ti−O and Ti sites than only the Ti−O site, a linear relationship as observed for both sites was expected. However, a balance between Ti and Ti−O sites is required for effective chain growth probabilities. We must admit that to grow the carbon chain the Ti site and Ti−O are mutually inclusive. However, a higher Ti number results in a significant decrease in the site time yield because of a higher acid site number as observed from TiO_2 calcined at 100 °C.

In addition, the possible role of Ti Lewis acidity in the formation of the intermediate is examined by correlating the formation rates of products with the vicinal Ti Lewis acidic sites and O−H stretching vibration of oxygen sites in Figure 3c,d. The formation rates of cyclic ketone (2,3,4,5-tetramethyl-2-cyclopenten-1-one) and C_9 hydrocarbons (2-ethyl-5,5-dimethyl-1,3-cyclopentadiene and 2,4-dimethyl-1-heptene) increase almost linearly with increasing number of the vicinal Ti Lewis acid sites before it reaches 0.26 mmol/g_{cat}, while the rate correlates poorly with the O−H stretching vibration of the oxygen site. In addition, the site number of O−H stretching vibration of the oxygen site is much smaller (almost 1/10) than that of vicinal Ti Lewis acidic sites. It suggests that the vicinal Ti Lewis acid sites catalyze the dehydration and cyclization reactions (formation of cyclic ketone) and the hydrogenation−dehydration reaction (formation of hydrocarbon from oxygenates), which is in good agreement with the literature.[44,55,56] However, a further increase in the vicinal Ti Lewis acid site led to a slight decrease in the site time yield of cyclic ketone and hydrocarbons. This is because the acidic strength is weaker on TiO_2 calcined at 100 °C (Figure 2). The maximum activity corresponds to TiO_2 calcined at 350 °C.

Based on the above results, the reaction pathway for the C_9-cyclic ketone formation from propanal was proposed (Scheme 2). The kinetic relevant steps for the formation of C_9-cyclic ketone can be classified into three steps: step (a), adsorption and removal of alpha hydrogen to form enolate; step (b), surface C−C coupling reaction between enolate (C_3 and C_6) and adsorbed propanal; step (c), rapid cyclization of aldol-derived species into C_9-cyclic ketone in the presence of H_2 and Cu/SiO_2-TiO_2. The proposed steps a and b are similar to those reported by Iglesia et al.[12] In step 1 and step 2 in Scheme 2, the enolate formation involving abstraction of acidic hydrogen at the alpha position was indicated as the kinetic relevant step in the aldol condensation reaction.[10] Our DFT calculation (Figure 3e) reveals that the electronegative oxygen (−0.07 eV) in propanal adsorbed on the Lewis acidic site of Ti and the basic site of adjunct O could attract the alpha hydrogen. The Ti site aided in the stabilization of the adsorbed enolate, which is consistent with the experimental observation where the activation of propanal requires Lewis acid and base pairs (Ti−O), as shown in Scheme 2.

Scheme 2. Possible Reaction Pathways for the Carbon Coupling Reaction between C_6 Alkanal and Propanal To Yield C_9-Cyclic Ketone

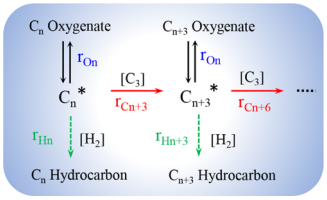

Moreover, this phenomenon explains well that the chain growth activity depends not only on the Ti−O and Ti site numbers but also on the Ti−O and Ti site strength. High basicity of the site is preferred, and a lower basic strength of Ti−O results in a lower attraction ability of alpha hydrogen and thus a lower activity. In addition, a relatively strong Ti Lewis acidic site stabilizes the adsorbed species better. In steps b and c, the Ti and Ti−O site pairs are required for the C−C coupling through the surface reaction between enolate and alkanals (C_{3+}). The basic site of O in Ti−O is saturated by H after the activation of propanal, which allows adsorption of propanal on the vicinal Ti site (step c in Scheme 2). Adsorption of propanal activates the α carbon and promotes the C−C coupling reaction between the adsorbed enolate and propanal. This forms aldol species (3-hydroxy-2-methylpentanal), while the vicinal Ti sites catalyze the dehydration of H_2O in the C_6 condensation intermediate and release basic site (steps 4 and 5 in Scheme 2). The O in the OH group of 3-hydroxy-2-methylpentanal adsorbed on the Lewis acidic site of Ti, and the basic site of adjunct O could attract the alpha hydrogen, which promotes dehydration (steps 6 and 7 in Scheme 2). Desorption of water and products from Ti−O and Ti finalized the catalytic cycle. The Ti acidic sites are required for the adsorption of C_6 alkenal and thereby stabilize the

https://dx.doi.org/10.1021/acssuschemeng.0c02200
ACS Sustainable Chem. Eng. 2020, 8, 9434−9446

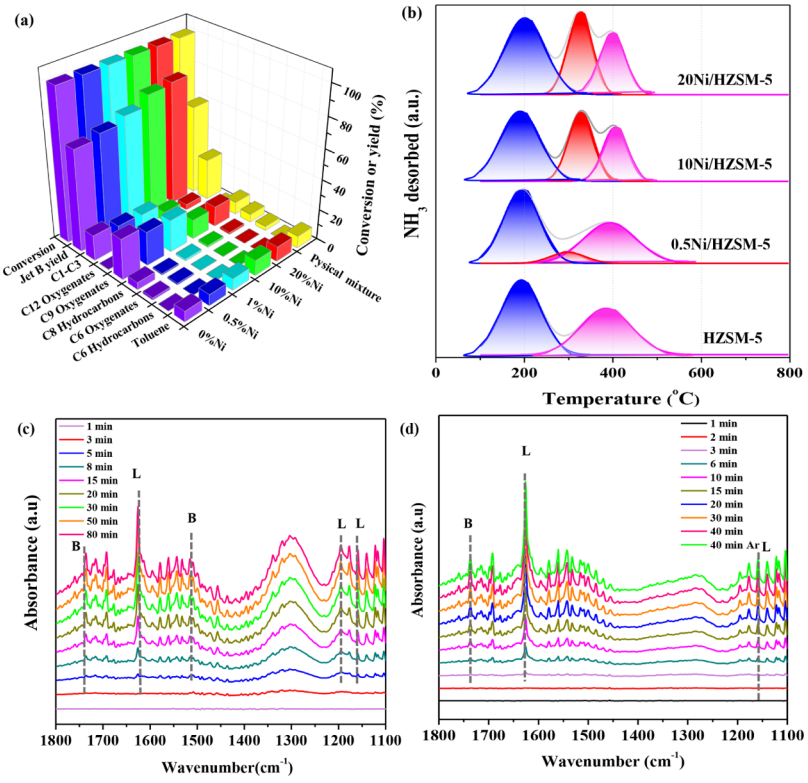

Figure 4. Effects of Ni loading on 5 wt %Cu/SiO_2 (0.5 g)−TiO_2 (350 °C; 0.5 g)||Ni/HZSM-5 (1 g) product yield (a). Reaction conditions: 1/WHSV of 5.2 h based on the total weight of the catalyst, the hydrogen pressure of 0.39 bar, the propanal pressure of 0.21 bar, the temperature of 300 °C, and the total pressure of 1.0 bar, and the Ni loading for the physical mixture is 20 wt %; NH_3-TPD spectra for different Ni/HZSM-5 catalysts (b); DRIFTS spectra of absorbed NH_3 on (c) HZSM-5 and (d) 20Ni/HZSM-5 catalysts exposed to a flow of 500 ppm NH_3/Ar (50 mL/min) at 150 °C for different times.

enolate for chain growth. In step c, the formed C_6, 2-methyl-2-pentenal, adsorbs on the Lewis acid sites (k_9), where the Ti−O and Ti sites aid in the reaction between C_3-enolate and the adsorbed C_6, yielding C_9 alkanal via aldol condensation reaction (steps 10−13 in Scheme 2). Furthermore, the final product is formed on the Lewis acid sites via methyl transfer and isomerization to C_9-cyclic ketone via 1−5 ring closure on the Lewis acidity. It has been reported that it is easy to cleave ethyl groups than the methyl group based on the stability of the carbonium ions.[57] Therefore, the vicinal Ti site redraws electrons from the oxygen via an electrophilic attack. This aids in the trans-alkylation/isomerization reaction toward 2,3,4,5-tetramethyl-2-cyclopenten-1-one. C_9 alkanal quickly undergoes cyclization to form a C_9-cyclic ketone ($C_9H_{14}O$) and significantly terminates the chain growth via the vicinal Ti^{4+} site.

Active Sites for Hydrodeoxygenation of Cyclic Ketone Intermediate to Aromatics. The tandem reactions were studied using a dual-bed (upstream: Cu/SiO_2−TiO_2|| downstream: Ni/HZSM-5) catalyst in a single packed bed reactor to convert the cyclic ketones to aromatics. It is found that jet fuel range aromatics (C_7−C_{12}) are the dominating products, and detailed product distribution is tabulated in Tables S1−S7. The relationship between the Ni content and product yield is indicated in Figure 4a. In terms of net jet fuel range aromatic formation, the downstream Ni/HZSM-5 catalyst is more active than HZSM-5. The site requirements and reaction mechanism for the conversion of C_9 ketone to aromatics were examined by altering the bifunctionality (metal−acid site) via increasing the Ni content on HZSM-5. The addition of Ni on HZSM-5 in the downstream increased the formation of aromatics. The best jet fuel range aromatic yield of 81.7% was obtained over the 20 wt % Ni/HZSM-5 catalyst.

To probe the effects of Ni loading on the formation of aromatics from C_9-cyclic ketone, the acidic properties of HZSM-5 and 20% Ni/HZSM-5 catalysts were studied by NH_3-DRIFTS and NH_3-TPD, respectively. In Figure 4c,d, the bands at 1153, 1255, and 1624 cm^{-1} are ascribed to Lewis acid sites, while 1519 and 1734 cm^{-1} are attributed to Brønsted acid sites.[54,58] NH_3-TPD was then used to quantify the number and strength of the Lewis and Brønsted sites (Figure 4b). The amount of absorbed NH_3 increases with exposure time for both HZSM-5 and Ni/HZSM-5. However, the impregnation of Ni on HZSM-5 led to the disappearance of the Brønsted peak at 1464 cm^{-1}. This indicates that some of the Brønsted protons have been selectively replaced by Ni ions. NH_3-TPD spectra of HZSM-5, 0.5Ni/HZSM-5, 10Ni/HZSM-5, and 20Ni/HZSM-5 are shown in Figure 4b. Two peaks are observed on HZSM-5, where the peak at 200−220 °C is ascribed to physisorbed NH_3 and that at 400−420 °C is ascribed to the Brønsted acidity, while no visible Lewis acid sites were observed in the NH_3-TPD thermogram.[59,60] In contrast, three peaks are observed at 200, 350, and 420 °C for Ni-impregnated samples.[61] The newly formed 350 °C peak based on the deconvolution is associated with Lewis acidic sites because of Ni modification; however, similar peaks have been assigned to Ni species in accordance with previous reports.[61] The total acidity increases with higher Ni loading on the support (HZSM-5), which is similar to the previous report

https://dx.doi.org/10.1021/acssuschemeng.0c02200
ACS Sustainable Chem. Eng. 2020, 8, 9434−9446

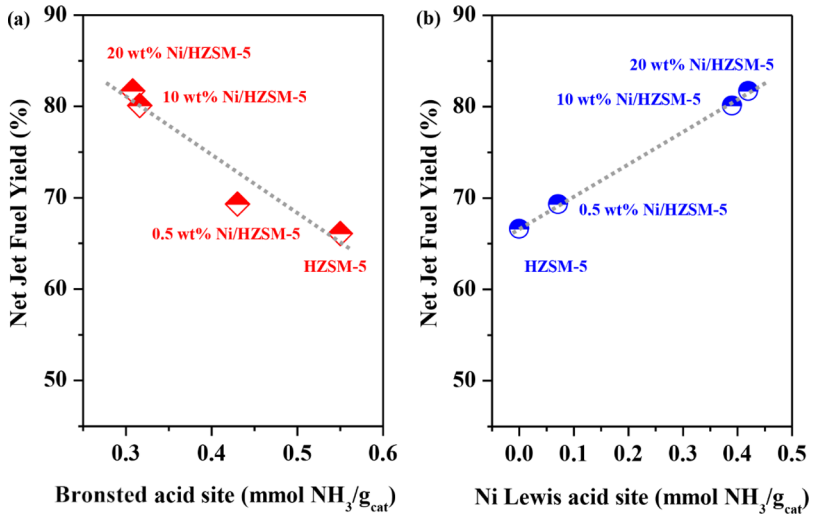

Figure 5. Relationship between Brønsted acid sites (a) and Lewis acid sites (b) to the jet fuel range hydrocarbon yield for HZSM-5, 0.5, 10 and 20 wt % Ni/HZSM-5, (0.5 g) Cu/SiO_2-(0.5 g) TiO_2–Ni/ZSM-5 (1 g). Reaction conditions: 1/WHSV of 5.2 h, a hydrogen pressure of 0.39 bar, a propanal pressure of 0.21 bar, a temperature of 300 °C, a total pressure of 1.0 bar, and a TOS of 12 h.

Scheme 3. Reaction Mechanism for Hydrogenation–Dehydration and Aromatization Chain Reactions on the Downstream Bed Catalyst (Ni/HZSM-5)

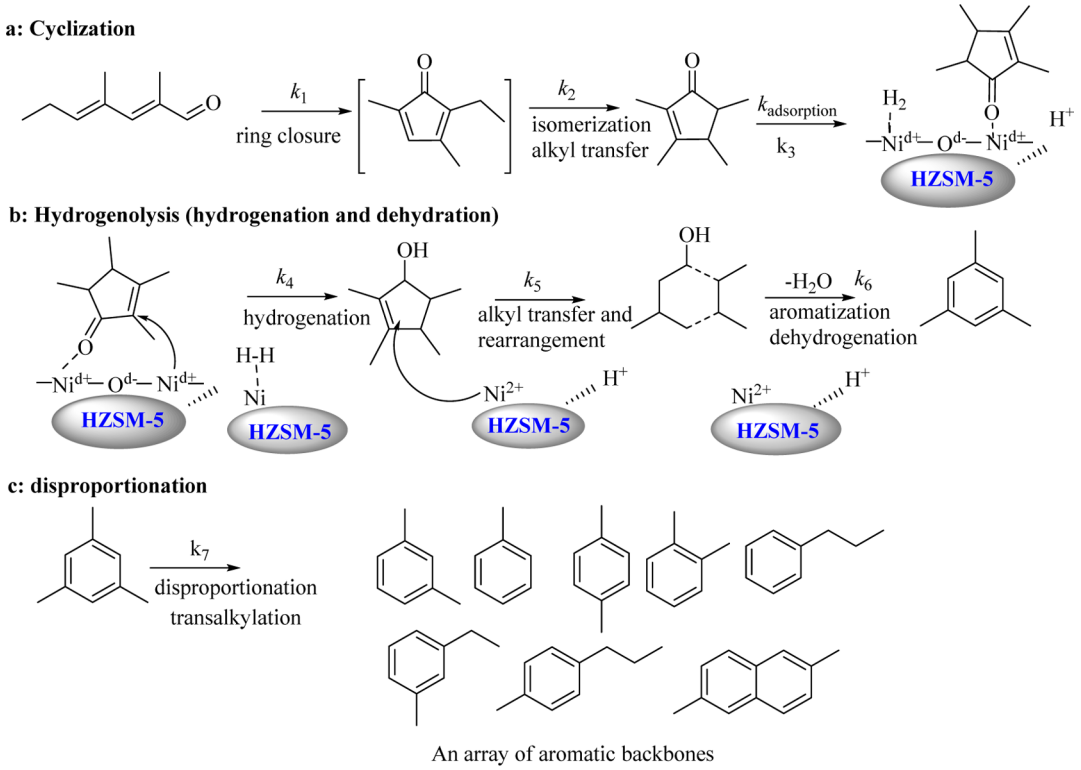

on Zn/HZSM-5.[62,63] The increase in the Ni loading results in the 45.5% decline in the Brønsted sites at 20 wt % Ni loading, suggesting that Ni selectively occupies some Brønsted acidic sites.

The effects of the inherent Brønsted acidity and the induced Lewis acidity were correlated with the jet fuel range hydrocarbon yield. Figure 5 shows the relationship between Brønsted acid sites and Lewis acid sites to the net jet fuel range aromatic yield obtained through tuning Ni loading. HZSM-5 catalyzes the reactions toward aromatics. The jet fuel yield decreases linearly with more Brønsted acid sites (Figure 5a), while the jet fuel yield correlates positively with the Lewis sites as the Ni loading increases (Figure 5b). These results indicate that the Lewis acid created by the addition of Ni mainly contributed to the enhanced activity for hydrogenation as well as possibly dehydration and aromatization reactions. In this sequence reaction, the C_9-cyclic intermediate possibly undergoes hydrogenation from the reduced Ni sites and further dehydration from the acidic Lewis sites.[9] On the zeolites with higher Ni loading, a larger number of Lewis acid sites, a smaller number of Brønsted sites, and a higher jet fuel yield suggest a much higher activity over the Ni-added catalyst compared to

https://dx.doi.org/10.1021/acssuschemeng.0c02200
ACS Sustainable Chem. Eng. 2020, 8, 9434–9446

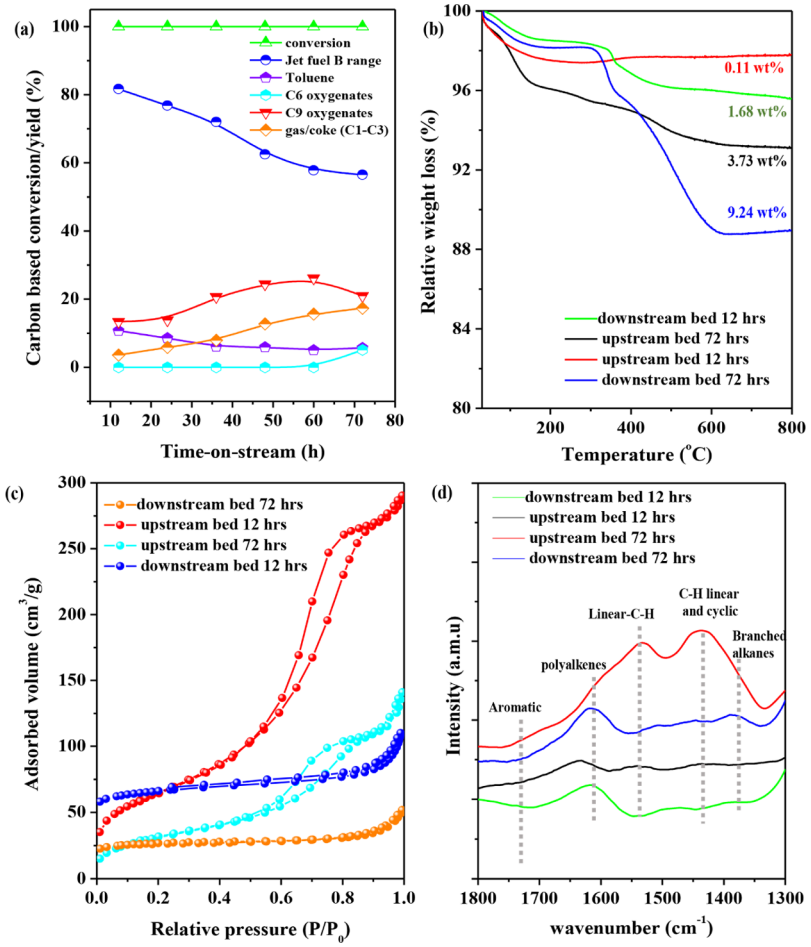

Figure 6. Stability analysis (a) and regeneration (in situ reduction at the reaction temperature) after 72 h on 5 wt % Cu/SiO_2-TiO_2 (350 °C)||20 wt % Ni/ZSM-5 as a function of time on stream; TGA (b); N_2 physisorption (c); and FT-IR spectra (d) for the 12 and 72 h spent catalyst. Reaction conditions: 1/WHSV of 5.2 h, a pressure of hydrogen 0.39 bar, a pressure of propanal 0.21 bar, a total pressure of 1.0 bar, and a temperature of 300 °C.

neat HZSM-5. Meanwhile, the Brønsted sites (possible activator for dehydration and hydrogen-transfer reaction[64]) have few hydrogenation−dehydrogenation sites for the hydrogenolysis toward the aromatic formation, and thus, a lower jet fuel yield is observed on HZSM-5 as compared to that on Ni/HZSM-5. Herein, the bifunctional sites including Brønsted sites from HZSM-5 and Lewis acidic sites formed via Ni modification of the designed catalyst facilitated the jet fuel range hydrocarbon generation.

The possible reaction pathway toward aromatization catalyzed by Ni/HZSM-5 is proposed in Scheme 3. The mechanistic pathway for the conversion of C_9-cyclic ketone to an array of aromatics (C_7-C_{12}) is based on observed products (Tables S1−S7) via tuning Ni loading. The C_9-linear alkanal is not detected but reported as the main intermediate for the formation of C_1-C_5 ring closure (k_1).[7] This leads to the formation of another intermediate, 2-ethyl-3,5-dimethyl-cyclopentene-2,4-dione, which further undergoes isomerization and alkyl transfer (k_2) to the stable product, 2,3,4,5-tetramethyl-2-cyclopenten-1-one, referred herein to as C_9-cyclic ketone. The C_9-cyclic intermediate for jet fuel range aromatic generation is quite similar to the results of Zhang et al. where jet fuel range C_8-C_9 aromatic hydrocarbons were synthesized in high carbon yield using C_9 isophorone as a feedstock.[65] In the presence of hydrogen and Ni/HZSM-5, there is H_2 adsorption and H_2 spillage (k_3), followed by C_9-cyclic ketone hydrodeoxygenation to aromatics (mesitylene) via hydrogenation (k_4), dehydration (k_5), and isomerization (k_6) chain reactions. The formed mesitylene further undergoes disproportionation, alkyl transfer, and isomerization to xylene isomers and other alkylated aromatics (k_7). These reactions (dehydration, isomerization, and aromatization) are mainly promoted by the hydrogenation Ni site, Lewis acidic sites, and possibly Brønsted acidity (H^+). The presence of Ni on HZSM-5 enhances the performance compared with that on pure HZSM-5.

Stability Analysis of the Dual-Bed System. The formation of a jet fuel over the dual-bed catalyst system was studied for 72 h period over the Cu/SiO_2-TiO_2||20 wt % Ni/ZSM-5 catalyst, as shown in Figure 6. The mass balance for all experiments is greater than 90%. Compared with the reported state-of-the-art HZSM-5 catalyst which has a sharp decline in activity, the dual-bed catalyst exhibited much better performance, that is, an almost 100% conversion over 72 h period. However, there is still an increase in C_9 oxygenates with a gradual decrease in the jet fuel range aromatic yield. Based on the above analysis, the C_9 intermediate cannot be successfully converted to aromatics, indicating that the deactivation is on the downstream Ni/HZM-5 catalyst. Furthermore, multi-techniques such as TGA, N_2 physisorption, FT-IR, and

https://dx.doi.org/10.1021/acssuschemeng.0c02200
ACS Sustainable Chem. Eng. 2020, 8, 9434−9446

HRTEM were used to confirm the deactivation mechanism of the downstream bed catalyst. In Figure 6a, the relative weight loss from 130 to 600 °C represents the coke formation from 12 h for the Ni/HZSM-5 catalyst. Meanwhile, the coke content observed for the downstream bed (Ni/HZSM-5) at 12 h and 72 h is 1.68 and 9.24 wt %, respectively. In addition, the accessible surface area of the downstream Ni/HZSM-5 catalyst has a 59% reduction in the BET surface area from 224 to 83 m^2/g (Table S8). The pore volume also declines from 0.14 to 0.07 cm^3/g, indicating a 50% decay. The reduction of pore volume should be due to coke formation, causing pore-blocking deactivation. FT-IR was further used to investigate the properties of the hydrocarbon deposits on the spent catalyst. For the downstream catalyst, a band is observed at 1600−1650 cm^{-1} at 12 h, which is assigned to polyalkenes. In addition, branched alkanes are also observed at ca. 1380 cm^{-1}. Therefore, the coke for the downstream catalyst might be mainly polyalkenes and branched alkane. Similar spectra are observed for 12 and 72 h, but the signal for 72 h was more intense. Moreover, the average Ni particle increases from 11 and 26 nm, as confirmed by the TEM results (Figure S3).

It can also be seen from Figure 6 that there is an increase in the C_6 oxygenate pool yield together with the reduction of C_9 oxygenates, which indicates the slight deactivation of the upstream Cu/SiO_2-TiO_2 catalyst. This also clearly demonstrates that the propanal is converted to C_6 and then C_9 intermediate for subsequent jet fuel production. The mass of coke or accumulated intermediates on the upstream bed (Cu/SiO_2-TiO_2) at 72 h is 3.73 wt %. Compared with the downstream bed catalyst, this smaller coke content for upstream bed catalysts could be possibly due to its lower acid sites. In addition, the coke causes the reduction of surface area from 228 to 108 m^2/g and the 55% decrease of pore volume from 0.43 to 0.19 cm^3/g (Table S9). The coke properties are analyzed by FT-IR. At 72 h, there are two broad bands at 1400−1450 and 1500−1550 cm^{-1}, representing C−H linear together with cyclic/linear C−H asymmetric stretching. Without bifunctionality, the coke of the upstream bed catalyst is conceivably by the intermediates ($\alpha-\beta$ unsaturated carbonyl polymerization). In addition, there is also Cu aggregation from 22 to 30 nm. Although the dual-bed Cu/SiO_2-TiO_2||Ni/ZSM-5 catalyst suffers from deactivation, it still shows the highest catalytic stability compared with the reported results.[8,22,23] This analysis of performance and deactivation offers a promising avenue for the further enhancement of the catalytic performance for jet fuel range hydrocarbon synthesis from light oxygenates.

CONCLUSIONS

In this work, jet fuel range hydrocarbon is produced from biomass-derived light alkanal in a single tubular reactor with the dual-bed catalyst system, and a high yield of 81.7% and a purity of 85% have been achieved. It is found that the required kinetic steps such as enolate formation and surface chain growth reactions are activated by Ti−O site pairs and Ti sites. The combined Ti−O and −Ti structure is required during the surface reaction step. This site is originated from the combination of Ti−O and vicinal Lewis acid center from Ti. TiO_2 passivation at 350 °C gives an optimum C_9-cyclic ketone yield because of relatively balanced Ti and Ti−O site count as well as an intermediate acid/base strength. Furthermore, the active site for hydrodeoxygenation of the C_9-cyclic ketone to jet fuel range aromatics involves hydrogenation−dehydration and aromatization chain reaction on Ni/HZSM-5. Thus, increasing Ni loading led to a remarkable enhancement in the jet fuel yield. These active site requirements are also demonstrated by the time-based analysis of catalytic performance. This work is significant to the design of an efficient dual-bed catalyst for the generation of jet fuel range hydrocarbons from various biomass-derived light oxygenates.

ASSOCIATED CONTENT

Supporting Information

The Supporting Information is available free of charge at https://pubs.acs.org/doi/10.1021/acssuschemeng.0c02200.

Characterizations of dual-bed catalysts and detailed product distributions at different reaction conditions (PDF)

AUTHOR INFORMATION

Corresponding Author

De Chen − *Department of Chemical Engineering, Norwegian University of Science and Technology, Trondheim 7491, Norway;* orcid.org/0000-0002-5609-5825; Email: de.chen@ntnu.no

Authors

Isaac Yeboah − *Department of Chemical Engineering, Norwegian University of Science and Technology, Trondheim 7491, Norway*

Xiang Feng − *Department of Chemical Engineering, Norwegian University of Science and Technology, Trondheim 7491, Norway; State Key Laboratory of Heavy Oil Processing, China University of Petroleum, Qingdao 266580, China;* orcid.org/0000-0001-7299-5690

Gang Wang − *School of Chemical Engineering, East China University of Science and Technology, Shanghai 200237, China*

Kumar Ranjan Rout − *SINTEF Industry, Trondheim 7465, Norway*

Zhenping Cai − *Department of Chemical Engineering, Norwegian University of Science and Technology, Trondheim 7491, Norway*

Xuezhi Duan − *School of Chemical Engineering, East China University of Science and Technology, Shanghai 200237, China;* orcid.org/0000-0002-5843-5950

Xinggui Zhou − *School of Chemical Engineering, East China University of Science and Technology, Shanghai 200237, China*

Complete contact information is available at: https://pubs.acs.org/10.1021/acssuschemeng.0c02200

Author Contributions

I.Y. and X.F. contributed equally to this work. The manuscript was written through contributions of all authors. All authors have given approval to the final version of the manuscript.

Notes

The authors declare no competing financial interest.

ACKNOWLEDGMENTS

The support from Research Council of Norway (243749 of ENERGIX program and 267648 of BIA program), National Natural Science Foundation of China (21978325), and Norwegian University of Science and Technology is highly acknowledged.

REFERENCES

(1) Huber, G. W.; Iborra, S.; Corma, A. Synthesis of transportation fuels from biomass: Chemistry, catalysts, and engineering. *Chem. Rev.* **2006**, *106*, 4044−4098.

(2) Venkatakrishnan, V. K.; Delgass, W. N.; Ribeiro, F. H.; Agrawal, R. Oxygen removal from intact biomass to produce liquid fuel range hydrocarbons via fast-hydropyrolysis and vapor-phase catalytic hydrodeoxygenation. *Green Chem.* **2015**, *17*, 178−183.

(3) Huber, G. W.; Corma, A. Synergies between bio- and oil refineries for the production of fuels from biomass. *Angew. Chem., Int. Ed.* **2007**, *46*, 7184−7201.

(4) Rahman, M. M.; Liu, R.; Cai, J. Catalytic fast pyrolysis of biomass over zeolites for high quality bio-oil − A review. *Fuel Process. Technol.* **2018**, *180*, 32−46.

(5) Bergem, H.; Xu, R.; Brown, R. C.; Huber, G. W. Low temperature aqueous phase hydrogenation of the light oxygenate fraction of bio-oil over supported ruthenium catalysts. *Green Chem.* **2017**, *19*, 3252−3262.

(6) Griffin, M. B.; Iisa, K.; Wang, H.; Dutta, A.; Orton, K. A.; French, R. J.; Santosa, D. M.; Wilson, N.; Christensen, E.; Nash, C.; Van Allsburg, K. M.; Baddour, F. G.; Ruddy, D. A.; Tan, E. C. D.; Cai, H.; Mukarakate, C.; Schaidle, J. A. Driving towards cost-competitive biofuels through catalytic fast pyrolysis by rethinking catalyst selection and reactor configuration. *Energy Environ. Sci.* **2018**, *11*, 2904−2918.

(7) Lin, F.; Chin, Y.-H. Mechanism of intra- and inter-molecular C=C bond formation of propanal on brønsted acid sites contained within MFI zeolites. *J. Catal.* **2014**, *311*, 244−256.

(8) Gangadharan, A.; Shen, M.; Sooknoi, T.; Resasco, D. E.; Mallinson, R. G. Condensation reactions of propanal over $Ce_xZr_{1-x}O_2$ mixed oxide catalysts. *Appl. Catal., A* **2010**, *385*, 80−91.

(9) Poole, O.; Alharbi, K.; Belic, D.; Kozhevnikova, E. F.; Kozhevnikov, I. V. Hydrodeoxygenation of 3-pentanone over bifunctional pt-heteropoly acid catalyst in the gas phase: Enhancing effect of gold. *Appl. Catal., B* **2017**, *202*, 446−453.

(10) Kunkes, E. L.; Gürbüz, E. I.; Dumesic, J. A. Vapour-phase C-C coupling reactions of biomass-derived oxygenates over $Pd/CeZrO_x$ Catalysts. *J. Catal.* **2009**, *266*, 236−249.

(11) Gürbüz, E. I.; Kunkes, E. L.; Dumesic, J. A. Dual-bed catalyst system for C-C coupling of biomass-derived oxygenated hydrocarbons to fuel-grade compounds. *Green Chem.* **2010**, *12*, 223−227.

(12) Wang, S.; Goulas, K.; Iglesia, E. Condensation and esterification reactions of alkanals, alkanones, and alkanols on TiO_2: Elementary steps, site requirements, and synergistic effects of bifunctional strategies. *J. Catal.* **2016**, *340*, 302−320.

(13) Di Cosimo, J. I.; Díez, V. K.; Apesteguía, C. R. Base catalysis for the synthesis of α,β-unsaturated ketones from the vapor-phase aldol condensation of acetone. *Appl. Catal., A* **1996**, *137*, 149−166.

(14) Zhao, L.; An, H.; Zhao, X.; Wang, Y. TiO_2-catalyzed n-valeraldehyde self-condensation reaction mechanism and kinetics. *ACS Catal.* **2017**, *7*, 4451−4461.

(15) Young, Z. D.; Hanspal, S.; Davis, R. J. Aldol Condensation of acetaldehyde over titania, hydroxyapatite, and magnesia. *ACS Catal.* **2016**, *6*, 3193−3202.

(16) Roelofs, J. C. A. A.; Lensveld, D. J.; van Dillen, A. J.; de Jong, K. P. On the structure of activated hydrotalcites as solid base catalysts for liquid-phase aldol condensation. *J. Catal.* **2001**, *203*, 184−191.

(17) Aramendía, M. a. A.; Borau, V.; Jiménez, C.; Marinas, A.; Marinas, J. M.; Ruiz, J. R.; Urbano, F. J. Magnesium-containing mixed oxides as basic catalysts: base characterization by carbon dioxide TPD−MS and test reactions. *J. Mol. Catal. A: Chem.* **2004**, *218*, 81−90.

(18) Zhao, C.; Lercher, J. A. Upgrading pyrolysis oil over Ni/HZSM-5 by cascade reactions. *Angew. Chem.* **2012**, *124*, 6037−6042.

(19) Iliopoulou, E. F.; Stefanidis, S. D.; Kalogiannis, K. G.; Delimitis, A.; Lappas, A. A.; Triantafyllidis, K. S. Catalytic upgrading of biomass pyrolysis vapors using transition metal-modified ZSM-5 Zeolite. *Appl. Catal., B* **2012**, *127*, 281−290.

(20) Lin, F.; Zhang, J.; Liu, D.; Chin, Y.-H. C. Cascade reactions in tunable lamellar micro- and mesopores for C=C bond coupling and hydrocarbon synthesis. *Angew. Chem.* **2018**, *130*, 13068−13072.

(21) Lin, F.; Chin, Y.-H. Alkanal transfer hydrogenation catalyzed by solid brønsted acid sites. *J. Catal.* **2016**, *341*, 136−148.

(22) Zhu, X.; Lobban, L. L.; Mallinson, R. G.; Resasco, D. E. Tailoring the mesopore structure of HZSM-5 to control product distribution in the conversion of propanal. *J. Catal.* **2010**, *271*, 88−98.

(23) Hoang, T. Q.; Zhu, X.; Sooknoi, T.; Resasco, D. E.; Mallinson, R. G. A comparison of the reactivities of propanal and propylene on HZSM-5. *J. Catal.* **2010**, *271*, 201−208.

(24) Ramasamy, K. K.; Gerber, M. A.; Flake, M.; Zhang, H.; Wang, Y. Conversion of biomass-derived small oxygenates over HZSM-5 and its deactivation mechanism. *Green Chem.* **2014**, *16*, 748−760.

(25) Müller, S.; Liu, Y.; Vishnuvarthan, M.; Sun, X.; van Veen, A. C.; Sanchez-Sanchez, M.; Lercher, J. A.; Lercher, J. A. Coke formation and deactivation pathways on H-ZSM-5 in the conversion of methanol to olefins. *J. Catal.* **2015**, *325*, 48−59.

(26) Gou, M.-L.; Cai, J.; Song, W.; Liu, Z.; Ren, Y.-L.; Pan, B.; Niu, Q. Coking and deactivation behavior of ZSM-5 during the isomerization of styrene oxide to phenylacetaldehyde. *Catal. Commun.* **2017**, *98*, 116−120.

(27) Henkelman, G.; Arnaldsson, A.; Jónsson, H. A fast and robust algorithm for bader decomposition of charge density. *Comput. Mater. Sci.* **2006**, *36*, 354−360.

(28) Sanville, E.; Kenny, S. D.; Smith, R.; Henkelman, G. Improved grid-based algorithm for bader charge allocation. *J. Comput. Chem.* **2007**, *28*, 899−908.

(29) Wang, S.; Iglesia, E. Experimental and theoretical assessment of the mechanism and site requirements for ketonization of carboxylic acids on oxides. *J. Catal.* **2017**, *345*, 183−206.

(30) Ma, S.; Sadakiyo, M.; Heima, M.; Luo, R.; Haasch, R. T.; Gold, J. I.; Yamauchi, M.; Kenis, P. J. A. Electroreduction of carbon dioxide to hydrocarbons using bimetallic Cu-Pd catalysts with different mixing patterns. *J. Am. Chem. Soc.* **2017**, *139*, 47−50.

(31) Dhas, N. A.; Raj, C. P.; Gedanken, A. Synthesis, characterization, and properties of metallic copper nanoparticles. *Chem. Mater.* **1998**, *10*, 1446−1452.

(32) Li, L.; Yan, J.; Wang, T.; Zhao, Z.-J.; Zhang, J.; Gong, J.; Guan, N. Sub-10 nm rutile titanium dioxide nanoparticles for efficient visible-light-driven photocatalytic hydrogen production. *Nat. Commun.* **2015**, *6*, 5881.

(33) Yue, W.; Zhou, W. Porous crystals of cubic metal oxides templated by cage-containing mesoporous silica. *J. Mater. Chem.* **2007**, *17*, 4947−4952.

(34) Melligan, F.; Hayes, M. H. B.; Kwapinski, W.; Leahy, J. J. Hydro-pyrolysis of biomass and online catalytic vapor upgrading with Ni-ZSM-5 and Ni-MCM-41. *Energy Fuels* **2012**, *26*, 6080−6090.

(35) Wu, C.; Wang, L.; Williams, P. T.; Shi, J.; Huang, J. Hydrogen production from biomass gasification with Ni/MCM-41 catalysts: Influence of Ni content. *Appl. Catal., B* **2011**, *108-109*, 6−13.

(36) Markovits, A.; Fahmi, A.; Minot, C. A theoretical study of CO_2 adsorption on TiO_2. *Theochem* **1996**, *371*, 219−235.

(37) León, M.; Díaz, E.; Bennici, S.; Vega, A.; Ordónez, S.; Auroux, A. J. I.; research, e. c. Adsorption of CO_2 on hydrotalcite-derived mixed oxides: Sorption mechanisms and consequences for adsorption irreversibility. *Ind. Eng. Chem. Res.* **2010**, *49*, 3663−3671.

(38) Tumuluri, U.; Howe, J. D.; Mounfield, W. P., III; Li, M.; Chi, M.; Hood, Z. D.; Walton, K. S.; Sholl, D. S.; Dai, S.; Wu, Z. Effect of surface structure of TiO_2 nanoparticles on CO_2 adsorption and SO_2 resistance. *ACS Sustainable Chem. Eng.* **2017**, *5*, 9295−9306.

(39) Li, H.; Jiao, X.; Li, L.; Zhao, N.; Xiao, F.; Wei, W.; Sun, Y.; Zhang, B. Synthesis of glycerol carbonate by direct carbonylation of glycerol with CO_2 over solid catalysts derived from Zn/Al/La and Zn/Al/La/M (M = Li, Mg and Zr) hydrotalcites. *Catal. Sci. Technol.* **2015**, *5*, 989−1005.

(40) Köck, E.-M.; Kogler, M.; Bielz, T.; Klötzer, B.; Penner, S. In situ FT-IR spectroscopic study of CO_2 and CO adsorption on Y_2O_3, ZrO_2, and Yttria-stabilized ZrO_2. *J. Phys. Chem. C* **2013**, *117*, 17666−17673.

https://dx.doi.org/10.1021/acssuschemeng.0c02200
ACS Sustainable Chem. Eng. 2020, 8, 9434−9446

(41) Collins, S. E.; Baltanás, M. A.; Bonivardi, A. L. Infrared spectroscopic study of the carbon dioxide adsorption on the surface of Ga_2O_3 polymorphs. *J. Phys. Chem. B* **2006**, *110*, 5498−5507.
(42) Faba, L.; Díaz, E.; Ordóñez, S. Aqueous-phase furfural-acetone aldol condensation over basic mixed oxides. *Appl. Catal., B* **2012**, *113-114*, 201−211.
(43) Yang, X.; Zhao, B.; Zhuo, Y.; Gao, Y.; Chen, C.; Xu, X. Drifts study of ammonia activation over CaO and sulfated CaO for NO reduction by NH_3. *Environ. Sci. Technol.* **2011**, *45*, 1147−1151.
(44) Peña, D. A.; Uphade, B. S.; Smirniotis, P. G. TiO_2-supported metal oxide catalysts for low-temperature selective catalytic reduction of NO with NH_3: I. Evaluation and characterization of first row transition metals. *J. Catal.* **2004**, *221*, 421−431.
(45) Álvarez, M. G.; Chimentão, R. J.; Figueras, F.; Medina, F. Tunable basic and textural properties of hydrotalcite derived materials for transesterification of glycerol. *Appl. Clay Sci.* **2012**, *58*, 16−24.
(46) Alvarez, M. G.; Segarra, A. M.; Contreras, S.; Sueiras, J. E.; Medina, F.; Figueras, F. Enhanced use of renewable resources: Transesterification of glycerol catalyzed by hydrotalcite-like compounds. *Chem. Eng. J.* **2010**, *161*, 340−345.
(47) Wang, L.; Ma, Y.; Wang, Y.; Liu, S.; Deng, Y. Efficient synthesis of glycerol carbonate from glycerol and urea with lanthanum oxide as a solid base catalyst. *Catal. Commun.* **2011**, *12*, 1458−1462.
(48) Di Cosimo, J. I.; Acosta, A.; Apesteguía, C. R. Allylic alcohol synthesis by gas-phase hydrogen transfer reduction of unsaturated ketones. *J. Mol. Catal. A: Chem.* **2005**, *234*, 111−120.
(49) Li, C.; Sakata, Y.; Arai, T.; Domen, K.; Maruya, K.-i.; Onishi, T. Carbon monoxide and carbon dioxide adsorption on cerium oxide studied by Fourier-transform infrared spectroscopy. Part 1.—Formation of carbonate species on dehydroxylated CeO_2, at room temperature. *J. Chem. Soc., Faraday Trans. 1* **1989**, *85*, 929−943.
(50) Li, C.; Sakata, Y.; Arai, T.; Domen, K.; Maruya, K.-i.; Onishi, T. Adsorption of carbon monoxide and carbon dioxide on cerium oxide studied by Fourier-transform infrared spectroscopy. Part 2.—Formation of formate species on partially reduced CeO_2 at room temperature. *J. Chem. Soc., Faraday Trans. 1* **1989**, *85*, 1451−1461.
(51) Yu, J.-G.; Yu, H.-G.; Cheng, B.; Zhao, X.-J.; Yu, J. C.; Ho, W.-K. The effect of calcination temperature on the surface microstructure and photocatalytic activity of TiO_2 thin films prepared by liquid phase deposition. *J. Phys. Chem. B* **2003**, *107*, 13871−13879.
(52) Tumuluri, U.; Howe, J. D.; Mounfield, W. P., III; Li, M.; Chi, M.; Hood, Z. D.; Walton, K. S.; Sholl, D. S.; Dai, S.; Wu, Z. Effect of surface structure of TiO_2 nanoparticles on CO_2 adsorption and SO_2 resistance. *ACS Sustainable Chem. Eng.* **2017**, *5*, 9295−9306.
(53) Bou-Orm, N.; Iorgu, A.; Daniele, S.; Guilhaume, N. Modification of acid−base properties of TiO_2 by Nb and Mg dopants: Influence on the activity of Pd−Cu/(Mg, Nb)−TiO_2 catalysts for nitrate hydrogenation. *Appl. Catal., A* **2013**, *467*, 414−420.
(54) Lai, S.; Meng, D.; Zhan, W.; Guo, Y.; Guo, Y.; Zhang, Z.; Lu, G. The promotional role of Ce in Cu/ZSM-5 and in situ surface reaction for selective catalytic reduction of NO_x with NH_3. *RSC Adv.* **2015**, *5*, 90235−90244.
(55) Kim, Y. T.; Jung, K.-D.; Park, E. D. Gas-phase dehydration of glycerol over ZSM-5 catalysts. *Microporous Mesoporous Mater.* **2010**, *131*, 28−36.
(56) González, J.; Wang, J. A.; Chen, L.; Manríquez, M.; Salmones, J.; Limas, R.; Arellano, U. Quantitative determination of oxygen defects, surface lewis acidity, and catalytic properties of mesoporous MoO_3/SBA-15 catalysts. *J. Solid State Chem.* **2018**, *263*, 100−114.
(57) Santilli, D. The mechanism of aromatic transalkylation in ZSM-5. *J. Catal.* **1986**, *99*, 327−334.
(58) Bin, F.; Song, C.; Lv, G.; Song, J.; Wu, S.; Li, X. Selective catalytic reduction of nitric oxide with ammonia over zirconium-doped copper/ZSM-5 catalysts. *Appl. Catal., B* **2014**, *150-151*, 532−543.
(59) Rodríguez-González, L.; Hermes, F.; Bertmer, M.; Rodríguez-Castellón, E.; Jiménez-López, A.; Simon, U. The acid properties of H-ZSM-5 as studied by NH_3-TPD and ^{27}Al-MAS-NMR spectroscopy. *Appl. Catal., A* **2007**, *328*, 174−182.
(60) Al-Dughaither, A. S.; de Lasa, H. HZSM-5 zeolites with different SiO_2/Al_2O_3 ratios. characterization and NH_3 desorption kinetics. *Ind. Eng. Chem. Res.* **2014**, *53*, 15303−15316.
(61) Huang, J.; Chen, J. Comparison of Ni_2p/SiO_2 and Ni/SiO_2 for hydrogenolysis of glycerol: A consideration of factors influencing catalyst activity and product selectivity. *Chin. J. Catal.* **2012**, *33*, 790−796.
(62) Fanchiang, W.-L.; Lin, Y.-C. Catalytic fast pyrolysis of furfural over H-ZSM-5 and Zn/H-ZSM-5 catalysts. *Appl. Catal., A* **2012**, *419-420*, 102−110.
(63) Zhang, Q.; Wang, T.; Li, B.; Jiang, T.; Ma, L.; Zhang, X.; Liu, Q. Aqueous phase reforming of sorbitol to bio-gasoline over Ni/HZSM-5 catalysts. *Appl. Energy* **2012**, *97*, 509−513.
(64) Weingarten, R.; Tompsett, G. A.; Conner, W. C.; Huber, G. W. Design of solid acid catalysts for aqueous-phase dehydration of carbohydrates: The role of lewis and brønsted acid sites. *J. Catal.* **2011**, *279*, 174−182.
(65) Chen, F.; Li, N.; Wang, W.; Wang, A.; Cong, Y.; Wang, X.; Zhang, T. Catalytic conversion of isophorone to jet-fuel range aromatic hydrocarbons over a MoO_x/SiO_2 catalyst. *Chem. Commun.* **2015**, *51*, 11876−11879.

https://dx.doi.org/10.1021/acssuschemeng.0c02200
ACS Sustainable Chem. Eng. 2020, 8, 9434−9446